

Tobacco cigarette smoking induces cerebrovascular dysfunction followed by oxidative neuronal injury with the onset of cognitive impairment

Journal of Cerebral Blood Flow & Metabolism
0(0) 1–18
© The Author(s) 2024
Article reuse guidelines:
sagepub.com/journals-permissions
DOI: 10.1177/0271678X241270415
journals.sagepub.com/home/jcbfm



Mohamed G Ewees¹, Mohamed A El-Mahdy¹,
Yousef Hannawi²  and Jay L Zweier¹ 

Abstract

While chronic smoking triggers cardiovascular disease, controversy remains regarding its effects on the brain and cognition. We investigated the effects of long-term cigarette smoke (CS) exposure (CSE) on cerebrovascular function, neuronal injury, and cognition in a novel mouse exposure model. Longitudinal studies were performed in CS or air-exposed mice, 2 hours/day, for up to 60 weeks. Hypertension and carotid vascular endothelial dysfunction (VED) occurred by 16 weeks of CSE, followed by reduced carotid artery blood flow, with oxidative stress detected in the carotid artery, and subsequently in the brain of CS-exposed mice with generation of reactive oxygen species (ROS) and secondary protein and DNA oxidation, microglial activation and astrogliosis. Brain small vessels exhibited decreased levels of endothelial NO synthase (eNOS), enlarged perivascular spaces with blood brain barrier (BBB) leak and decreased levels of tight-junction proteins. In the brain, amyloid- β deposition and phosphorylated-tau were detected with increases out to 60 weeks, at which time mice exhibited impaired spatial learning and memory. Thus, long-term CSE initiates a cascade of ROS generation and oxidative damage, eNOS dysfunction with cerebral hypoperfusion, as well as cerebrovascular and BBB damage with intracerebral inflammation, and neuronal degeneration, followed by the onset of impaired cognition and memory.

Keywords

Cerebrovascular disease, oxidative stress, nitric oxide, free radicals, inflammation

Received 3 January 2024; Revised 21 May 2024; Accepted 25 June 2024

Introduction

While chronic tobacco cigarette smoking (CS) triggers oxidant stress and cardiovascular disease; questions and controversy remain regarding its effects on the brain and cognition.^{1–8} Initial studies reported protective effects of smoking in dementia; however, subsequent epidemiological studies reported that CS increases the risk of neurodegeneration and cognitive impairment (CI).^{1,3,7,8} Neurocognitive disorders, ranging from mild cognitive impairment to dementia, constitute a major worldwide health problem.^{9,10} CI is associated with cerebrovascular dysfunction and oxidative stress.^{11,12} Cerebrovascular disease has also been linked with late-life dementia and neurodegenerative diseases (ND).^{13,14} However, the process and mechanisms by which CS affects neurocognitive function remain unclear. Therefore, there is a need for

studies of the effects of long-term CS on cerebrovascular and neuronal function in well controlled exposure models that mimic human use.

Cerebral blood flow is modulated by nitric oxide (NO). Cerebral hypoperfusion can be triggered by

¹Department of Internal Medicine, Division of Cardiovascular Medicine, Davis Heart & Lung Research Institute, College of Medicine, The Ohio State University, Columbus, Ohio, USA

²Division of Cerebrovascular Diseases and Neurocritical Care, Department of Neurology, College of Medicine, The Ohio State University, Columbus, Ohio, USA

Corresponding author:

Jay L Zweier, 420 West 12th Ave., TMRF 116A, Columbus, Ohio 43210, USA.

Email: jay.zweier@osumc.edu

vascular endothelial dysfunction (VED) with impaired endothelial NO synthase (eNOS)-mediated NO production and increased oxygen radical generation.¹⁵ Oxidative damage and vascular inflammation trigger VED with NOS dysfunction and uncoupling.^{16,17} This leads to the generation of superoxide and secondary reactive oxygen species (ROS) that react with NO to form reactive nitrogen species (RNS).¹⁸ VED can also impair blood-brain-barrier (BBB) integrity, enabling penetration of inflammatory cells or ROS (reactive oxygen species) from the blood stream into brain tissue, causing further oxidative damage and neuronal toxicity.^{19,20} Smoking-induced VED, with oxidative damage and vascular inflammation,²¹ is hypothesized to be a central cause of smoking-induced disease, including that affecting the central nervous system.^{22–24}

Cigarette smoke is a well-known source of free radicals and oxidative stress.^{1,25,26} The brain is highly vulnerable to oxidative damage that can cause or exacerbate the accumulation of amyloid β (A β) plaques, phosphorylated tau, and neurofibrillary tangles, which are central to the pathology of ND.^{27,28} Important questions remain regarding the effects of chronic CS exposure (CSE) and its secondary oxidant stress on the cerebral vasculature and whether this contributes to neuronal injury and CI. In this work, we hypothesized that the oxidants and toxic chemicals in cigarette smoke initiate a cascade of ROS generation and oxidative damage that leads to VED and cerebral hypoperfusion, along with cerebrovascular damage and inflammation, which together cause CI.

Therefore, we performed studies in a long-term mouse CSE model to measure the temporal progression of vascular changes and oxidative stress, as well as associated brain injury with altered cognition and memory. We observe that CSE causes ROS-mediated vascular damage, a known trigger of VED. Cerebrovascular damage occurs with decreased levels of BBB tight junction proteins and increased BBB permeability. Microglial activation and astrocytosis are seen in the brain with accumulation of A β and P-tau. With long-term exposure, these vascular and neuronal alterations progressively increase, associated with the onset of CI.

Material and methods

Materials

Chemicals, reagents, and other materials were from Millipore Sigma (Burlington) unless noted otherwise.

Animals and cigarette smoke exposure

Animals were housed in the animal care facility administered by the University Laboratory Animals

Resources Program (ULAR) of The Ohio State University and provided veterinary supervision of care. ULAR is accredited by the American Association for Accreditation of Laboratory Animal Care, and meets federal guidelines for the humane and appropriate care of laboratory animals, Federal Law (89–544, 91–579) and all NIH regulations enumerated in the NIH Guide for the Care and Use of Laboratory Animals (2011 edition). The experiments are reported in compliance with the Animals in Research: Reporting In Vivo Experiments (ARRIVE 2.0) guidelines.²⁹ Sixteen-week-old male C57/BL6 mice from Jackson Laboratory (Bar Harbor) were acclimatized for two weeks and randomly divided into air- and whole-body CS-exposed groups. CSE was performed according to the Massachusetts Intense Regimen Table, using 3R4F Kentucky research cigarettes. The smoking machine (TE-10, Teague Enterprises) was programmed to deliver one puff/min, 2 s puff duration, and 35 mL/puff volume into the 10 liter exposure chamber.²² Mice were exposed to four smoke cycles, each of 20 min. Each smoke cycle was followed by 10 minutes of filtered air. The total exposure was 120 min/day, five days/week for 60 weeks as described.³⁰ The smoke was diluted with filtered air to yield 250 mg/m³ of total suspended matter in the exposure chamber. Blood carboxyhemoglobin (CO-Hb) levels were measured spectrophotometrically immediately after exposure, with ~12% and <1% values for CS- and air-exposed mice, respectively. The exposure dose and protocol were designed to match typical human CSE as previously described.^{22,30} Plasma cotinine levels, measured immediately after exposure, were 79 ng/ml in CS-mice which is within the range detected in human smokers.³¹ In air-exposed mice, cotinine was undetectable. Temperature, humidity, O₂, CO₂, and CO levels in the exposure chamber were monitored during the exposure.³² The total time of exposure was 60 weeks. We measured the non-invasive parameters at 8, 16, 30, and 60 weeks for the temporal assessment of the vascular and cognitive changes. Most invasive measures in the brain or vascular tissues were limited to 16- and 60-week time points based on prior observations of disease pathogenesis in this mouse CSE model,^{22,30} for the detailed exposure protocol timeline see SI Figure S1. Body weight was measured at each time point see SI Figure S2. Consistent with previous reports, chronic smoking exposure in mice inhibits the normal gain of weight that occurs as a function of age.^{24,30}

Assessment of vascular reactivity of the carotid artery

Isolated mouse carotid artery vascular reactivity was measured as reported previously.²² Briefly, the carotid

artery was dissected from anaesthetized-heparinized mice, then placed in ice-cold modified Krebs-Henseleit buffer (KHB), cleaned and cut into rings of 2–3 mm length. Rings were mounted in a wire Myograph system-610M (Danish Myo-Technology, Ann Arbor, MI), using 5 ml organ baths filled with KHB maintained at 37°C that was continuously purged with 95% O₂–5% CO₂ gas. Following 1 hour of equilibration under a resting tension of 1 g, the responsiveness of each ring to *L*-phenylephrine (PE, 1 μM) was verified. Rings were then washed three times with KHB and allowed to relax for 30 min. For the experimental measurements, rings were pre-constricted with 1 μM PE, and then endothelial-dependent relaxation was measured from the concentration-dependent relaxation to acetylcholine (ACh). A steady level of relaxation following each ACh addition was achieved prior to adding the next concentration. The dose-response of vessel relaxation was expressed as percent decrease of PE-induced contraction. Endothelial-independent relaxation to sodium nitroprusside (SNP) was similarly measured. A PowerLab/8sp data acquisition system (AD Instruments, Sydney, Australia) with ADI Chart software (v 5.3) was used to record the changes in isometric tension.

Measurement of blood pressure

Blood pressure (BP) was measured by a non-invasive tail cuff using a CODA™ BP acquisition system (Kent Scientific Corp.) under isoflurane anesthesia.^{30,33} BP recordings were made twice weekly at weeks 8, 16, 30, and 60 of exposure.

Measurement of carotid blood flow and velocity

High-resolution ultrasound, combined with pulse-wave Doppler (Vevo 2100, Visual Sonic), was used to provide information on the carotid blood flow.³⁴ The image quality was optimized using the following parameters: Doppler Gain = 30 dB, Dynamic range = 35 dB, Doppler angle = 20°. Using the VevoLab 2.2.0 software (Visual Sonic), we measured the velocity profiles, velocity time integral (VTI), and the area of the carotid artery per cycle. Then, we calculated the blood flow volume using the equation: Flow volume = Carotid Area * VTI * HR.³⁴ Carotid bed vascular resistance (CVR) was calculated using the equation: CVR = (mean blood pressure)/(carotid blood flow).³⁵

Assays of malondialdehyde (MDA) and protein carbonyls (PC) in carotid artery homogenates

The OxiSelect™ MDA adduct and the OxiSelect™ protein carbonyl competitive ELISA kits (Cell Biolabs) were used according to the manufacturer's protocol.

Measurement of superoxide and nitric oxide generation

The brain was dissected, washed briefly with ice-cold PBS, frozen in Optimal Cutting Temperature (OCT; Tissue-Tek, Sakura Finetek, Inc.) embedding compound. Sections were incubated with dihydroethidium (DHE; 10 μM; Molecular Probes, Inc.) and the nuclear stain 4',6-Diamidino-2-phenylindole, dihydrochloride (DAPI; 1 μM) for 30 min at 37°C. Selected slides were pre-incubated with 100 μM of superoxide dismutase mimetic (SODm) manganese (III) tetra (4-benzoic acid) porphyrin chloride (MnTBAP) for 10 min prior to DHE to confirm specificity. At least four sections per animal were analyzed using ImageJ software.

For nitric oxide (NO) measurement, sections were incubated with the fluorescent dye 4,5-diaminofluorescein diacetate (DAF-2 DA; 5 μM) and DAPI (1 μM) in PBS for 30 min. In matched control experiments, sections were incubated with 100 μM of the specific NO scavenger, 2-Phenyl-4,4,5,5-tetramethylimidazole-1-oxyl-3-oxide (PTIO), for 10 min prior to DAF-2-DA to confirm specificity for NO. The slides were processed and analyzed as above.

Immunofluorescence imaging

The brain was fixed in 10% neutral buffered formalin for 24 hr, washed with PBS, dehydrated, sectioned at 5 μm thickness, and antigen retrieval performed. Mouse monoclonal antibodies used included 8-hydroxyguanosine (LifeSpan BioSciences Inc.), Aβ, P-tau, glial fibrillary acidic protein (GFAP), nitrotyrosine, ionized calcium binding adaptor molecule 1 (Iba1), albumin, fibrinogen, and CD31 (Proteintech, Rosemont), and rabbit polyclonal antibody against eNOS (Cell Signaling Technology), claudin-5 and occludin (Invitrogen). Secondary antibodies were Alexa Fluor 594 or 488 (Invitrogen). Anti-fade mounting media containing DAPI was added. Brain sections were digitally imaged and different fields were captured at 40× using a confocal microscope (FV3000 spectral confocal microscope, Tokyo, Japan). The microscope acquisition settings including excitation and emission wavelengths and irradiation power were adjusted to minimize auto-fluorescence background for the given fluorescent probe. At least four sections per animal were analyzed using ImageJ software.

Fluorescence staining of brain protein aggregates

The benzothiazole dye thioflavin S (ThioS) binds to amyloid aggregates and P-tau paired helical filaments with enhanced green fluorescence.^{36,37} Slides were incubated in ThioS solution for 10 min and sequentially rinsed with ethanol followed by distilled water.

Different fields were captured at 40× by confocal microscopy and analyzed as above.

Measurement of β amyloid in brain homogenate

Levels of A β 40 and A β 42 peptides in brain homogenate were measured using ELISA kit (Invitrogen), per the manufacturer's protocol.

Brain histological analysis

Histological analysis was performed from sections at the corpus callosum and hippocampus levels. Standard hematoxylin and eosin (H&E) staining was performed from processed paraffin blocks. Stained slides were examined for abnormalities of the capillaries and small vessels,³⁸ using Axioskop Widefield light microscopy (Carl Zeiss, Inc.).

Immunoblotting

The brain was dissected, washed with ice-cold heparinized PBS then snap-frozen. Frozen tissue was weighed, pulverized, and homogenized in ice-cold lysis buffer. Tissue homogenate was centrifuged at 15 K rpm for 20 min, supernatant was collected, and protein concentration was determined using the Bio-Rad DC kit. Cellular proteins from brain tissue homogenates were separated onto a gradient 4–20% SDS-polyacrylamide gel (Bio-Rad), and electro-blotted on a PVDF membrane. P-tau, and eNOS were detected using mouse monoclonal antibodies (1:200; Santa Cruz Biotechnology). Occludin and claudin-5 were detected using rabbit polyclonal antibodies (1:200; Invitrogen). A rabbit monoclonal antibody (1:1000; Cell Signaling Technology) was used to detect the loading control GAPDH. Membranes were incubated for 1 hr in a TBST buffer containing 5% non-fat dry milk to block non-specific binding. Primary antibodies were used in TBST buffer containing 1% non-fat dry milk overnight at 4°C. Membranes were washed with TBST, incubated with HRP-linked secondary antibodies (1:5000; Cell Signaling Technology) in 1% non-fat dry milk in TBST for 1 h at room temperature, and then washed three times, using TBST. Membranes were developed using the ECL Immunoblotting Detection Reagent (GE Healthcare). Protein bands were quantitated by measuring band intensity, compared to GAPDH band intensity, using ImageJ software. Full immunoblots with molecular weight markers are shown in supplementary Figures S5–S7.

Assessment of mouse cognitive function

Experiments were performed at the Ohio State University Neuroscience Rodent Behavior Core lab.

A single researcher, blinded to the animal groups, performed the following behavioral tests at 30 and 60 weeks of CSE and analyzed the data.

Barnes maze

Mouse spatial learning and memory were assessed as described.³⁹ Behavioral endpoints included: 1) Primary escape latency: defined as the time for a mouse to find the target hole and enter the escape tunnel; 2) Primary path length: defined as animal path lengths to reach the target hole; 3) Primary error: number of nose and head deflections made by a mouse into a non-target hole(s) before entering the escape tunnel; and 4) time in proximity: the time spent in the zone around the false-bottomed target hole.

Contextual and cued fear conditioning test

The ability of mice to learn and remember an association between environmental cues and aversive experiences was tested.⁴⁰ Freezing behavior, defined as complete immobility except breathing in response to fearful situations, was used as an index of associative fear learning and memory. VideoFreeze software (Med Associates Inc.) was used to quantify the mouse freezing behavior and activity.

Statistical analysis

Data are presented as mean \pm standard deviation (SD). The normal distribution of the data was assessed using the Shapiro-Wilk normality test; then, the statistical differences were assessed by performing unpaired t-test, 2-way ANOVA followed by Bonferroni multiple comparison test, or ANOVA with repeated measures for vessel relaxation data. GraphPad Prism software was used for analysis. Statistical differences were considered significant at $P < 0.05$.

Results

Cigarette smoke exposure causes hypertension, vascular endothelial dysfunction, and decreased carotid blood flow

As reported in our long-term CSE model,³⁰ systolic and diastolic blood pressure (BP) elevations occur as early as eight weeks of CSE, progressively increasing to 60 weeks (Figure 1(a) and (b)). Baseline BP values were similar in all animals, with values of 99 ± 9 mmHg for systolic BP (SBP) and 70 ± 9 mmHg for diastolic BP (DBP). At eight weeks of CSE, mice exhibited elevated BP, with SBP of 120 ± 16 mmHg and DBP of 87 ± 13 mmHg. BP progressively increased with 16, 30, and 60 weeks of exposure. At 60 weeks, marked

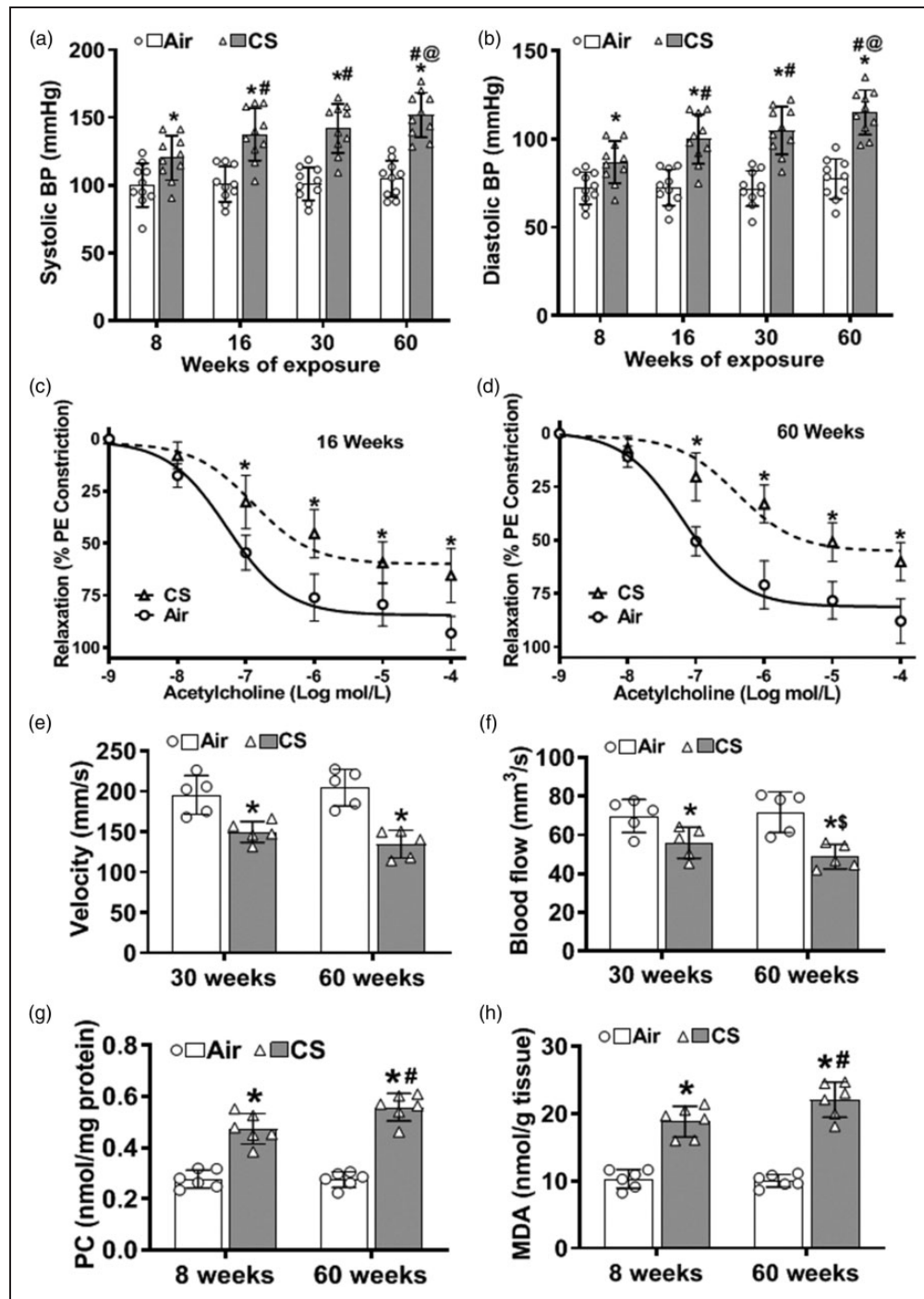


Figure 1. Cigarette smoke exposure causes vascular oxidative damage, hypertension, vascular endothelial dysfunction, and decreased carotid blood flow. (a–b) Eight weeks of cigarette smoke (CS) exposure elevated systolic and diastolic blood pressure (BP) with progressive increase out to 60 weeks, compared to air-exposed controls (Air). (c–d) Carotid artery rings were pre-constricted with 1 μ M phenylephrine (PE), and the concentration-dependent relaxation effect of acetylcholine was measured. 16 weeks of CS-exposure impaired vessel relaxation compared to Air, and this was more pronounced at 60 weeks. (e–f) Reduced carotid blood velocity and flow were seen with 30 weeks of CS exposure and further decreased with 60 weeks of exposure, compared to Air. (g–h) CS exposure caused time-dependent increase of protein carbonylation (PC) and malondialdehyde (MDA) levels in carotid artery homogenate, as measured by ELISA, compared to Air. Data are mean \pm SD with $n = 10$ for (a–b), $n = 6$ for (c–d), $n = 5$ for (e–f), and $n = 6$ for (g–h). Analysis for (a–b), and (e–h) was done by two-way ANOVA followed by Bonferroni multiple comparison test or ANOVA with repeated measures for (c–d). Data show statistical significance from: Air (*) at $p < 0.05$; or from 8 weeks (#), 16 weeks (@), and 30 weeks of CS exposure (\$) at $p < 0.05$.

hypertension (HTN) was present in CSE mice with SBP and DBP values of 151 ± 22 and 115 ± 16 mmHg. However, for the air-exposed mice, BP did not significantly change over time from 8 to 60 weeks of exposure, with values of 100 ± 6 and 104 ± 16 mmHg for SBP and 72 ± 13 and 77 ± 13 mmHg for DBP, respectively.

Since VED can contribute to HTN onset, we tested whether CSE impaired endothelial-mediated vascular relaxation. The relaxation of phenylephrine-pre-constricted carotid artery segments in response to the endothelium-dependent vasodilator acetylcholine (ACh) was evaluated at 8, 16, and 60 weeks of exposure. With eight weeks of exposure, only a slight insignificant impairment of ACh-induced relaxation was seen (data not shown). After 16 weeks of CSE, ACh-induced relaxation was significantly impaired, with a marked shift to the right in the dose-response curve (Figure 1(c)). With 60 weeks of exposure, further rightward shift was seen with blunted maximal relaxation (Figure 1(d)). Thus, CSE induced VED in an exposure-time-dependent manner. At 16 weeks, 50% relaxation was seen at 497 nM ACh compared to 57 nM in vessels from air-exposed controls. After 60 weeks of exposure, changes were more marked with shifts in the 50% relaxation values to 1004 nM in the CS-exposed group, compared to 92 nM with air exposure, respectively. Endothelial-independent relaxation to sodium nitropruside was also decreased but to a lesser extent than the alterations in ACh response (SI Figure S3).

Impaired vascular relaxation could lead to increased carotid tone and decreased carotid blood flow (CBF). To assess this, we measured *in vivo* carotid blood velocity (Figure 1(e)) and flow (Figure 1(f)). At thirty weeks of CSE, mice exhibited a 20% decrease in carotid blood velocity and a 23% decrease in carotid blood flow, with a further decrease at 60 weeks to 33% and 36%, respectively, of air-exposed control. No significant differences were seen at 8 or 16 weeks of exposure. The calculated carotid bed vascular resistance (CVR) in CS-exposed mice was increased to 2.3 ± 0.22 mmHg/s/mm³ at 30 weeks and further increased at 60 weeks to 2.8 ± 0.45 mmHg/s/mm³ in CS-exposed mice, compared to 1.2 ± 0.13 mmHg/s/mm³ and 1.3 ± 0.22 mmHg/s/mm³ in air-exposed mice, respectively (see SI Table 1).

Cigarette smoke exposure causes oxidative stress in the carotid artery

Since oxidative stress can trigger VED and subsequent HTN, we investigated whether CSE caused oxidative damage that preceded the onset of CI. Carotid artery homogenate was assayed for protein modification and lipid oxidation by ELISA. Elevated protein carbonyls (PC) and malondialdehyde (MDA) levels were detected as early as eight weeks of exposure. At eight weeks of

exposure PC (Figure 1(g)) and MDA (Figure 1(h)) levels were 0.47 ± 0.05 and 18.5 ± 2.4 nmol/g tissue, respectively, in CS-exposed mice, while in air-exposed controls values were 0.28 ± 0.02 and 10.1 ± 1.5 nmol/g tissue, respectively. The levels of these oxidative end products further increased at 60 weeks of CSE (Figure 1(g) and (h)).

Cigarette smoke exposure decreases endothelial eNOS expression and NO levels in the brain

Systemic VED can be caused by alterations in endothelial eNOS levels and its production of NO. Therefore, we measured the expression of eNOS in brain tissue by immunoblotting and immunohistology. While eNOS was clearly present and localized to brain vessels in air-control mice, eNOS levels were decreased following CSE. Immunoblotting showed a 45% decrease in eNOS (Figure 2(a) and (b)). Consistent with this, immunofluorescence microscopy showed a 50% decrease in eNOS in brain vessels (Figure 2(c) and (d)). With no primary eNOS antibody minimal fluorescence was seen, confirming the specificity of the observed fluorescence for eNOS (Figure 2(c), rightmost panel).

To further assess cerebrovascular eNOS function, NO levels were measured in brain vessels using the fluorescent probe DAF-FM. With CSE, the DAF-FM-derived fluorescence was ~60% decreased from the levels in air-exposed mice (Figure 2(e) and (f)). With addition of the NO scavenger, PTIO, the observed fluorescence was largely abolished confirming that it is NO-derived (Figure 2(e), right panel). Similarly in the absence of DAF-FM minimal if any fluorescence was seen.

Cigarette smoke exposure causes cerebrovascular injury with blood-brain barrier leak

Systemic vascular oxidative damage and dysfunction along with endothelial injury can lead to overall cerebrovascular dysfunction and BBB abnormalities. Therefore, we performed histopathological examination of the brain microvasculature. Changes were seen in small brain vessels of CS-exposed mice with enlarged perivascular space and congestion suggesting increased BBB leak. While in air-exposed mice, the cerebrovascular structure remained normal (Figure 3(a)). To further assess if CSE altered BBB permeability, the leak of the plasma proteins albumin and fibrinogen into the vessel wall and surrounding brain tissue was measured by immunohistology. The endothelial marker eNOS was used to demarcate the location and geometry of small vessels in the brain. Significant increases of albumin and fibrinogen were seen in surrounding vessels and the adjacent brain tissue of CS-exposed mice, indicating

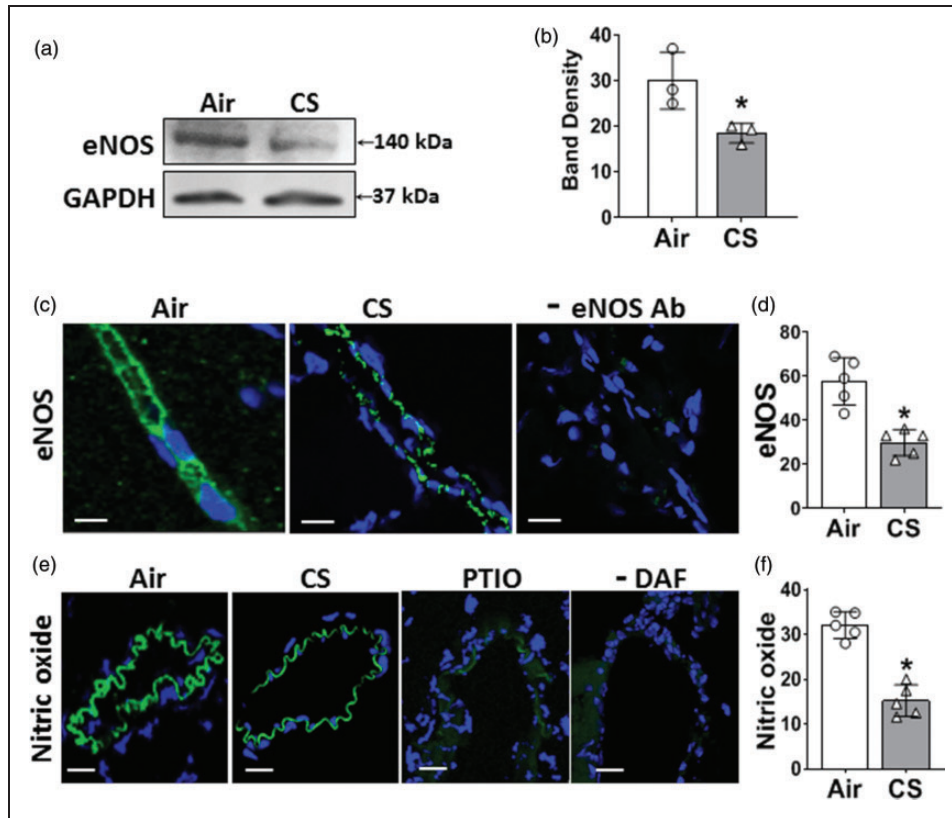


Figure 2. Cigarette smoke exposure decreases endothelial nitric oxide synthase (eNOS) and nitric oxide (NO) levels in the brain vessels and homogenate. Mice were exposed to cigarette smoke (CS) or filtered air (Air) for 60 weeks. (a) Western blotting measurement of eNOS in brain homogenate showing lower expression of eNOS in CS-exposed mice. (b) eNOS band density was quantitated and normalized to corresponding GAPDH bands. (c) Immunofluorescence staining of brain sections for eNOS (green) showing lower level in the brain vessels of CS-exposed mice compared to Air. DAPI (blue) was used to visualize the nuclei. A control in the absence of eNOS primary antibody is shown in the right panel. (d) Quantitation of eNOS fluorescence in (c). (e) Detection of NO in brain sections using DAF-FM fluorescent probe with brain vessels showing NO-derived green fluorescence. The right 2 panels show that the NO scavenger, PTIO, abolished the NO-derived fluorescence, while in the absence of DAF there was minimal background autofluorescence and (f) quantitation of NO-derived green fluorescence in (e). CS significantly decreased eNOS and NO levels in the brain, compared to Air. Scale bar (white line) is 20 μm with identical magnification in all panels. Data are mean \pm SD with $n = 3$ for (b), and $n = 6$ for (d) & (f). Analysis was done by unpaired t -test. *denotes significance from Air at $p < 0.05$.

BBB leakage (Figure 3(b) and (d)). Since BBB leak can be caused by alterations in the tight junction proteins Occludin and Claudin-5, we measured their expression in brain tissue from CS- or air-exposed mice. Levels of Occludin and Claudin-5 (Figure 3(c) and (e)) were decreased in brain vessels following CSE, to 62% and 55%, respectively, of those in air-exposed controls. Immunoblotting confirmed that CSE triggered a 2-fold decrease in the levels of these critical tight junction proteins (Figure 3(f) and (g)). Thus, chronic CSE caused BBB leak with downregulation of occludin and claudin-5.

Cigarette smoke exposure causes oxidative damage and ROS generation in the brain

Dysfunction in the BBB could trigger oxidative damage to the brain by facilitating the penetration of

CS-generated oxidants and ROS, together with endogenous inflammatory mediators. Therefore, we evaluated whether the observed CSE-induced vascular oxidative damage and alterations in eNOS expression and function were associated with increased oxidative stress and modifications in the brain of CS-exposed mice. In the brain, CSE-induced oxidative damage was seen as early as 16 weeks of exposure and became more severe at 60 weeks (Figure 4(a) to (h)). With 16 weeks of CSE, protein oxidation was increased with PC levels elevated to 194% and further increased at 60 weeks of CSE to 218% of those in air-controls. Lipid oxidation was also increased, with MDA levels elevated to 178% and 205% of those in air-controls at 16 and 60 weeks, respectively (Figure 4(a) and (b)).

Additional assays with imaging of superoxide and secondary ROS production in the brain were

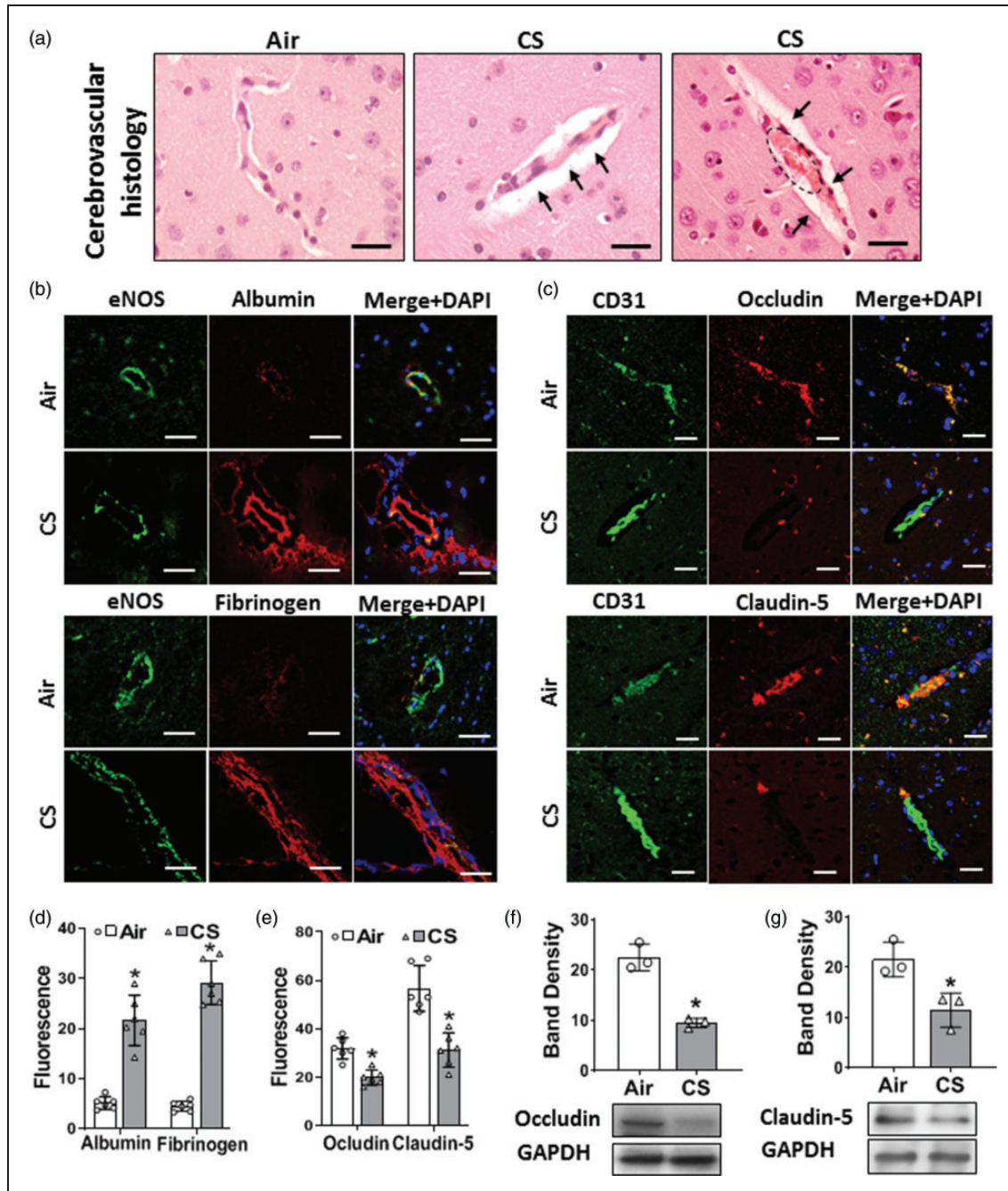


Figure 3. Cigarette smoke exposure causes cerebrovascular and blood-brain barrier (BBB) dysfunction. Mice were exposed to cigarette smoke (CS) or filtered air (Air) for 60 weeks. (a) Brain tissue was sectioned and stained with Haematoxylin & Eosin. Left photo shows normal vessel structures in Air, compared to enlarged perivascular space (black arrows in middle and right photos) and congested vessels (dotted circle in left photo) following CS exposure. Scale bar in black is 20 μ m with identical magnification in all panels. (b) Immunofluorescence staining of brain tissue. CS-exposed mice show increased extravasation of albumin and fibrinogen into the vessel wall and surrounding brain tissue. eNOS was used as an endothelial marker. Albumin and fibrinogen were co-localized with eNOS (Merge+DAPI). DAPI (blue) was used to visualize the nuclei. Scale bar in white is 20 μ m with identical magnification in all panels. (c) Immunofluorescence staining of brain tissue showing that CS decreased the levels of the BBB tight junction proteins Occludin and Claudin-5 in the endothelium of cerebral small vessels compared to Air. CD31 was used as an endothelial marker. Occludin and Claudin-5 were co-localized with CD31 (Merge+DAPI). DAPI (blue) was used to visualize the nuclei. Scale bar in white is 20 μ m with identical magnification in all panels. (d) Quantitation of Albumin and Fibrinogen fluorescence in (b). (e) Quantitation of Occludin, and Claudin-5 fluorescence in (c). (f-g) Western blotting showing decreased levels of Occludin (53 kDa) and Claudin-5 (22 kDa) in brain homogenate with band density quantitation and normalization to corresponding GAPDH bands. Data shown are mean \pm SD with $n = 6$ for (d-e) and $n = 3$ for (f-g). Analysis was done by unpaired t-test. *: denotes significance from Air at $p < 0.05$.

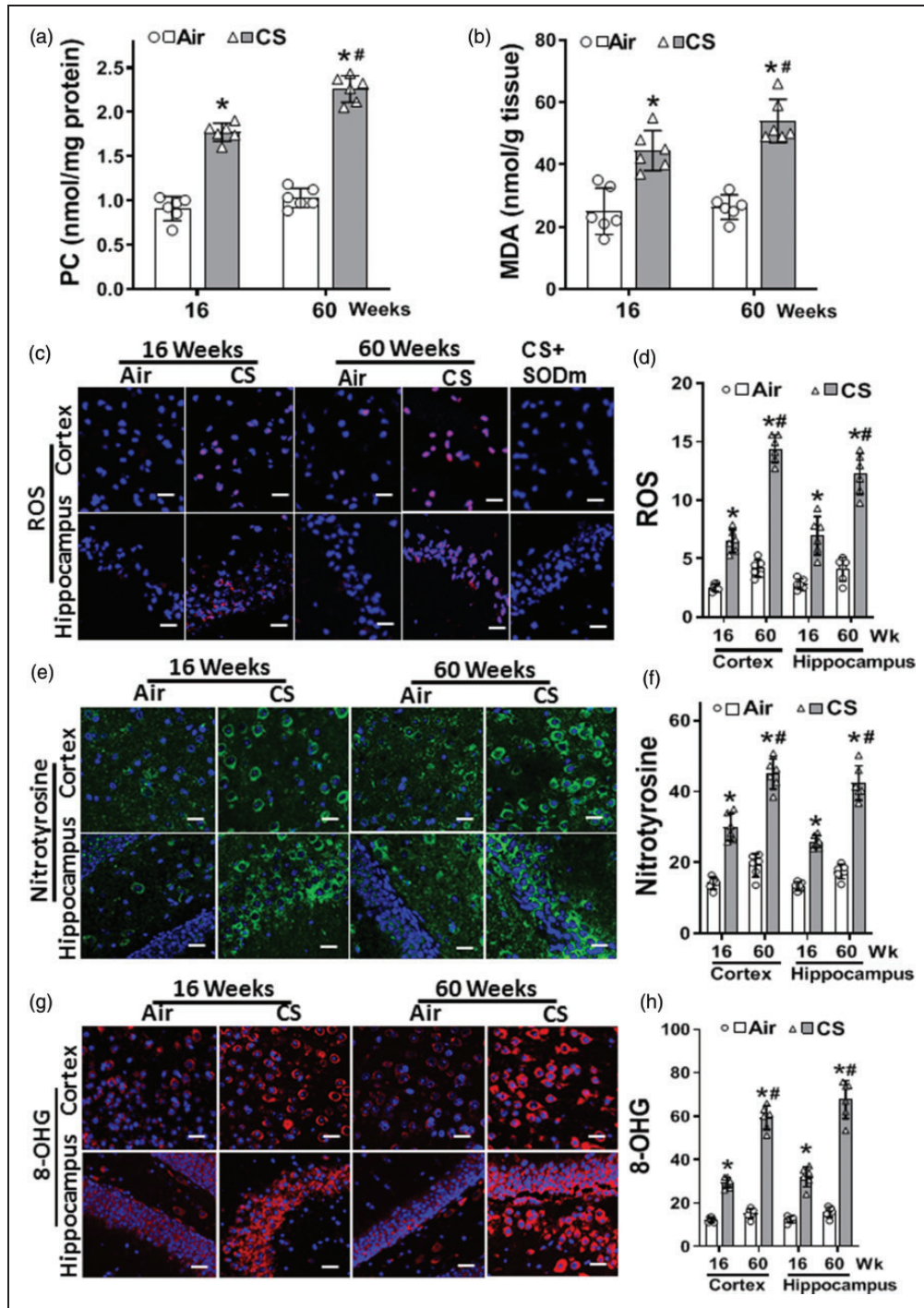


Figure 4. Cigarette smoke exposure causes reactive oxygen species generation and oxidative damage in the brain. Mice were exposed to cigarette smoke (CS) or filtered air (Air) for 16 or 60 weeks. (a–b) Show elevated levels of protein carbonyl (PC), and malondialdehyde (MDA) in CS-exposed mice as measured in brain homogenates by ELISA. (c) Sections of cortex and hippocampus show superoxide production (ROS; red), using dihydroethidium (DHE). Superoxide dismutase mimetic (SODm) was used to confirm the specificity of the DHE fluorescence from 60 weeks of CS exposure. Immunofluorescence staining of nitrotyrosine (e; green) and 8-hydroxyguanosine (g; 8-OHG; red). DAPI (blue) was used to visualize the nuclei. From series of experiments, fluorescence in (c), (e) & (g) were quantitated with data presented in (d), (f) & (h), respectively. CS increased PC and MDA levels in the brain with increased generation of ROS, nitrotyrosine, and 8-OHG in the cortex and hippocampus of 60 week CS-exposed mice; with similar but lower increase at 16 weeks of exposure. Scale bar shown corresponds to 50 μ m with identical magnification in all panels. Data are mean \pm SD with $n = 6$. Analysis was done by two-way ANOVA followed by Bonferroni multiple comparison test. Data show statistical significance from: Air (*); and 16 weeks of CS exposure (#) at $p < 0.05$.

performed using the fluorescence-based probe DHE, which is oxidized by superoxide to form the red fluorescent product 2-hydroxy ethidium.⁴¹ Increased red fluorescence to 257% or 245% of that in air-exposed controls was seen at 16 weeks of CSE in the cortex and hippocampus, respectively. These levels more than doubled at 60 weeks of CSE. (Figure 4(c) and (d)). In control experiments in the presence of the SODm Mn-TBAP this observed fluorescence was largely quenched (Figure 4(c)).

Superoxide and NO rapidly react to form the potent oxidant peroxynitrite that modifies tyrosine to form nitrotyrosine. Using a specific nitrotyrosine antibody, as seen from the green fluorescence, nitrotyrosine levels were increased at 16 weeks of CSE to 200% and 195% of air-control levels in the cortex and the hippocampus, respectively. Further increases in nitrotyrosine were seen at 60 weeks of exposure to 235% and 243% in the cortex and hippocampus, respectively (Figure 4(e) and (f)). Thus, CSE increased levels of superoxide generation and secondary ROS and RNS.

We further observed that CSE increased the DNA oxidation product 8-hydroxyguanosine (8-OHG) with

levels of 238% and 257% of those in air-control at 16 weeks of exposure in the cortex and hippocampus, respectively, with further increase after 60 weeks to 387% and 423%, respectively. Thus, CS-induced ROS and RNS increased oxidative DNA damage in the brain (Figure 4(g) and (h)).

Cigarette smoke exposure causes glial activation and astrocytosis in the brain

Cerebral oxidative stress and superoxide production could activate microglia, the brain resident macrophages, triggering neuro-inflammation. Common markers for microglial activation and astrocytosis include Iba1 and GFAP, respectively. Therefore, we measured the levels of these proteins in cortical and hippocampal brain sections. At 16 weeks, CSE increased Iba1 in the cortex to 164% of levels in air control, while at 60 weeks a 172% increase was seen (Figure 5(a) and (b)). GFAP increased in the cortex of CS-exposed mice to 224% and 363% of air-control levels (Figure 5(c) and (d)), at 16 and 60 weeks, respectively. Similarly, CSE increased the hippocampal levels

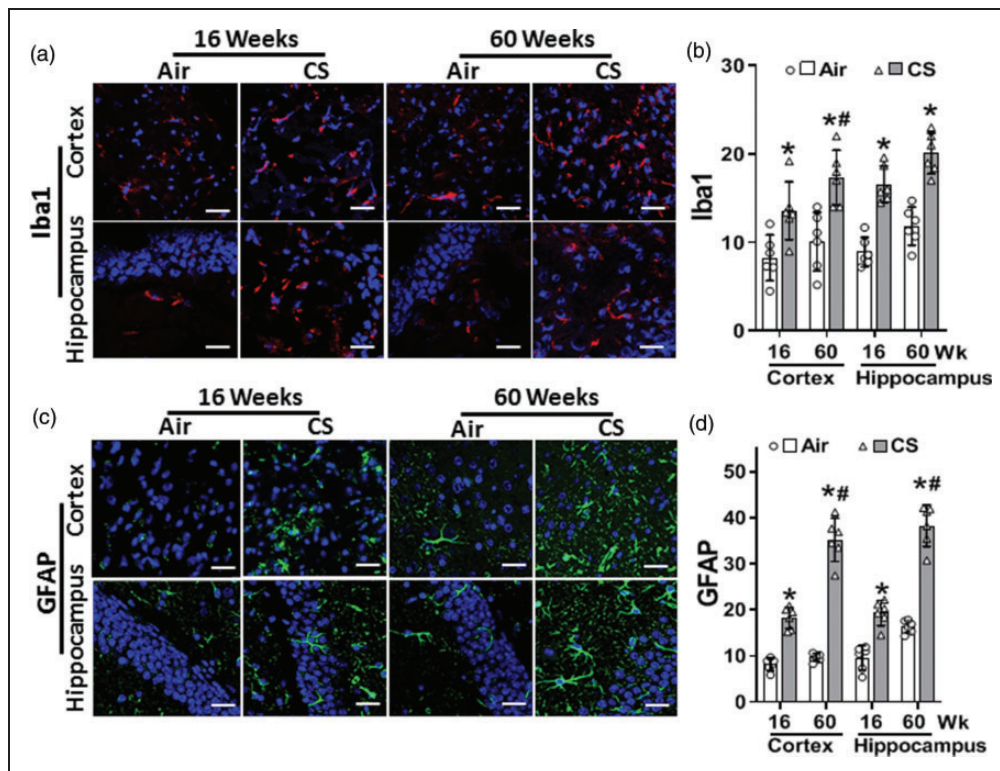


Figure 5. Cigarette smoke exposure increases microglial activation and astrocytosis in the brain. Mice were exposed to cigarette smoke (CS) or filtered air (Air) for 16 or 60 weeks. Brain sections were incubated with antibodies against microglial activation and astrocytosis markers Iba1 (a; red) and GFAP (c; green), respectively. DAPI (blue) was used to visualize the nuclei. Iba1 and GFAP images were analyzed, and fluorescence was quantitated and presented in (b) and (d), respectively. Scale bar corresponds to 50 μ m with identical magnification in all panels. Data are mean \pm SD with $n = 6$. Analysis was done by two-way ANOVA followed by Bonferroni multiple comparison test. Data show statistical significance from: Air (*) and 16 weeks of CS exposure (#) at $p < 0.05$.

of Iba1 to 186% and 170% of values in air-control at 16 and 60 weeks, respectively (Figure 5(a) and (b)). Hippocampal levels of GFAP were 200% and 236% of the air-control values (Figure 5(c) and (d) and SI Figure S4)) at 16 and 60 weeks, respectively. Thus, microglial activation and astrogliosis in the cortex and the hippocampus of CS-exposed mice increased from 16 to 60 weeks of exposure, demonstrating exposure duration-dependent induction of neuroinflammation.

Cigarette smoke exposure induces amylogenesis and tau phosphorylation in the brain

Since neuroinflammation and oxidative damage with alterations in BBB integrity may lead to amyloid pathology, immunohistology was performed to image the presence and location of A β in the brain. At 16 weeks, in the cortex and the hippocampus of CS-exposed mice, A β increased to 288% and 275% of the levels in air-exposed control, respectively, with a further increase to 352% and 432% of air-exposed control levels at 60 weeks (Figure 6(a) and (b)).

In order to confirm this, we measured the levels of A β peptides in brain sections by ELISA (Figure 6(c) and (d)). A β peptides 1–40 and 1–42 levels were increased in the brain of CS-exposed mice with values of 2.8 ± 0.5 and 0.3 ± 0.07 pg/mg tissue, respectively, compared to levels in air-exposed mice of 2.0 ± 0.2 and 0.17 ± 0.02 pg/mg tissue, respectively. Further increases were seen at 60 weeks with values of 4.1 ± 0.64 and 0.46 ± 0.12 pg/mg tissue, respectively, compared to 2.4 ± 0.37 and 0.24 ± 0.05 pg/mg tissue in air-exposed mice. The low A β levels in air-exposed controls, are comparable to reported values^{42,43} in control mice (Figure 6(c) and (d)). Thus, CSE triggered an increase in brain A β peptides.

Since inflammatory and oxidative neuronal injury may lead to elevations in P-tau levels, immunoblotting and immunohistology were performed to measure and image the effects of chronic CSE on P-tau. Immunoblotting of P-tau at 60 weeks in brain homogenate also showed a significant increase to 260% of levels in air-exposed control (Figure 6(e)). Immunohistology demonstrated that P-tau was increased to 213% or 196% of air-control levels in the cortex and the hippocampus, respectively, at 16 weeks of CSE (Figure 6(f) and (g)), with further increases to 297% and 303% of air-control levels at 60 weeks.

While no significant protein aggregates were seen in the cortex and the hippocampus of air-exposed mice, trace levels were detected at 16 weeks of CSE. At 60 weeks of CSE, prominent protein aggregates were seen with an increase to 413% of values in air-control, as measured by thioflavin-S fluorescence (Figure 6(h) and (i)). Thus, CSE resulted in amyloid and tau pathology

in the brain as early as 16 weeks of exposure that greatly increased by 60 weeks with the formation of protein aggregates.

Cigarette smoke exposure causes cognitive impairment

Since all the observed cerebrovascular and neuronal changes, especially amyloid deposition, and tau pathology, are associated with declines in cognition, we investigated whether CSE leads to CI. Cognitive and memory testing was performed with mice exposed to CS for 30 or 60 weeks. Mouse spatial learning and memory, along with associative fear learning and memory were evaluated using Barnes maze and fear conditioning tests, respectively (Figure 7). No significant changes were observed in both tests at 30 weeks of exposure. However, following 60 weeks, mouse spatial learning and memory were compromised. At 60 weeks of exposure, during the five days of the acquisition or learning phase, all mice showed no differences on the first trial day. However, air-exposed mice exhibited faster learning and better spatial memory from the second trial day than CS-exposed animals. CS-exposed mice demonstrated deficits in spatial learning and memory manifested by: 1) longer time for the mouse to find and enter the escape tunnel (Primary escape latency; Figure 7(a)); 2) longer path lengths taken to reach the target hole (Primary path length; Figure 7(b)); and 3) higher number of nose and head deflections made into the non-target hole(s) before entering the escape box (Number of primary errors; Figure 7(c)). On day eight (Probe trial or retention test), where the target hole is closed, with the escape tunnel and the escape box removed, mouse short-term memory was assessed by testing the animals' ability to recall the target hole and to stay in its vicinity. Air-exposed mice better identified the target hole than CS-exposed mice, remaining longer in the target hole vicinity. During the retention test, CS-exposed mice showed longer primary escape latency (Probe escape latency; Figure 7(d)) and longer primary path length (Probe path lengths; Figure 7(e)). CS-exposed mice also remained in the target hole's vicinity for a shorter time than air-exposed mice, indicating a memory deficit (Time in proximity; Figure 7(f)). Thus, spatial learning and memory was impaired after 60 weeks of CSE.

For the fear conditioning test, all mice were subjected to a fear conditioning session, and freezing response (fear behavior) to context and cued fear was tested in subsequent sessions. Freezing behavior during conditioning and testing was quantified. The percentage of time mice displayed freezing as a function of context or cued conditions was the same for 30 weeks of air or CSE (Figure 7(g)). However, both contextual

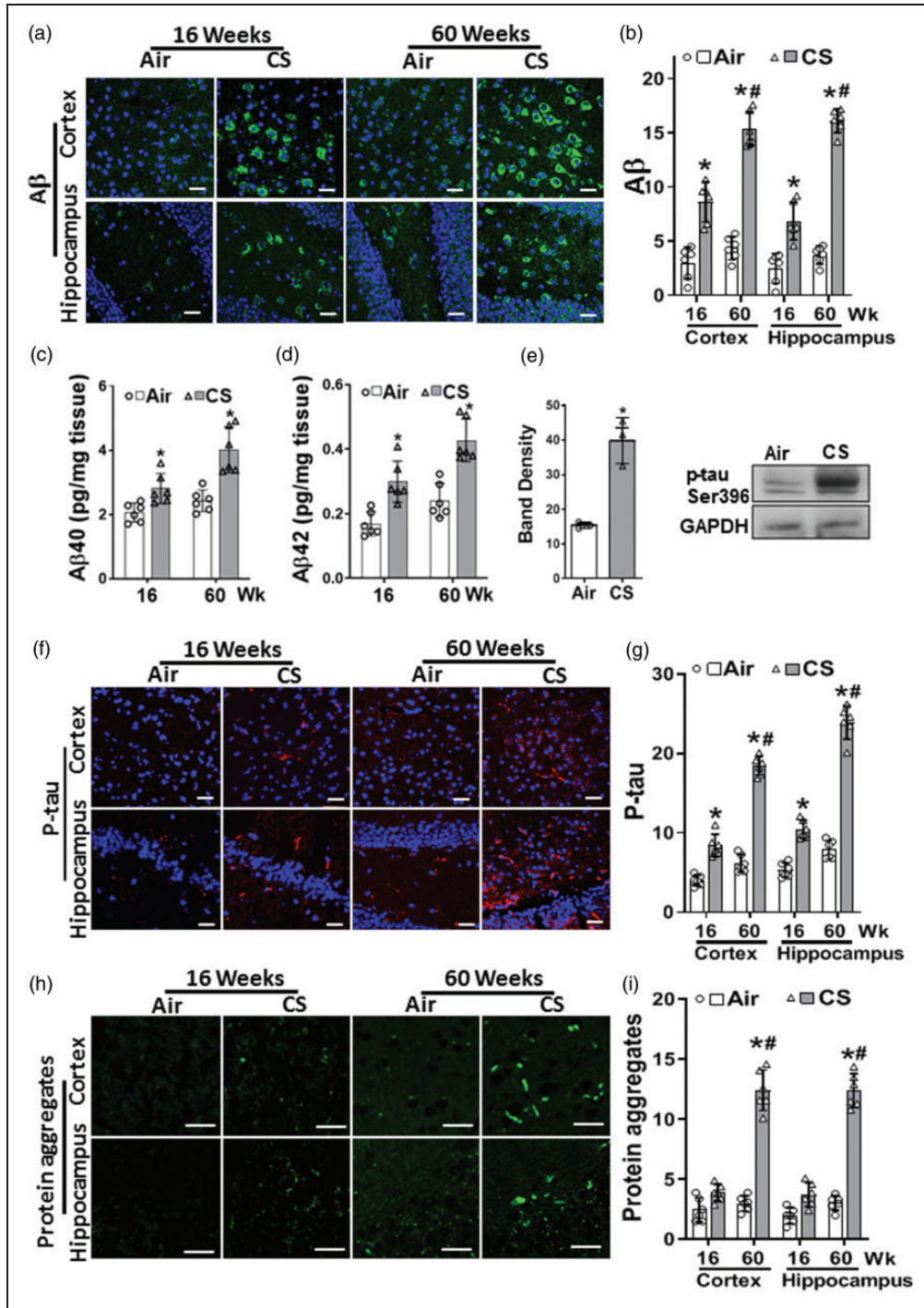


Figure 6. Cigarette smoke exposure induces amylogenes and tau phosphorylation in the brain. Mice were exposed to cigarette smoke (CS) or filtered air (Air) for 16 or 60 weeks. Sections from cortex and hippocampus were incubated with antibodies to amyloid β (a; A β ; green) or phosphorylated tau (f; P-tau; red). DAPI (blue) was used to visualize the nuclei. P-tau and A β images were analyzed, and fluorescence was quantitated and presented in (b) and (g), respectively. Amyloid fragments, A β 40 and A β 42, were quantitated in brain homogenate using ELISA (c) & (d), respectively. (e) Western blotting of P-tau (75 kDa) from brain homogenate of mice exposed to 60 weeks of CS or Air, with band density quantitation. (h) Protein aggregates (green) detected with Thioflavin S, with quantitation of the green fluorescence (i). CS caused a modest increase in p-tau and A β at 16 weeks, with greater elevation at 60 weeks that was accompanied by appearance of A β /p-tau protein aggregates. Scale bar corresponds to 50 μ m with all accompanying images in a panel shown at the same magnification. Data are means \pm SD with $n = 6$ for all panels except (e) with $n = 3$. Analysis was done by two-way ANOVA followed by Bonferroni multiple comparison test. Data show statistical significance from: Air (*) and 16 weeks of CS exposure (#) at $p < 0.05$.

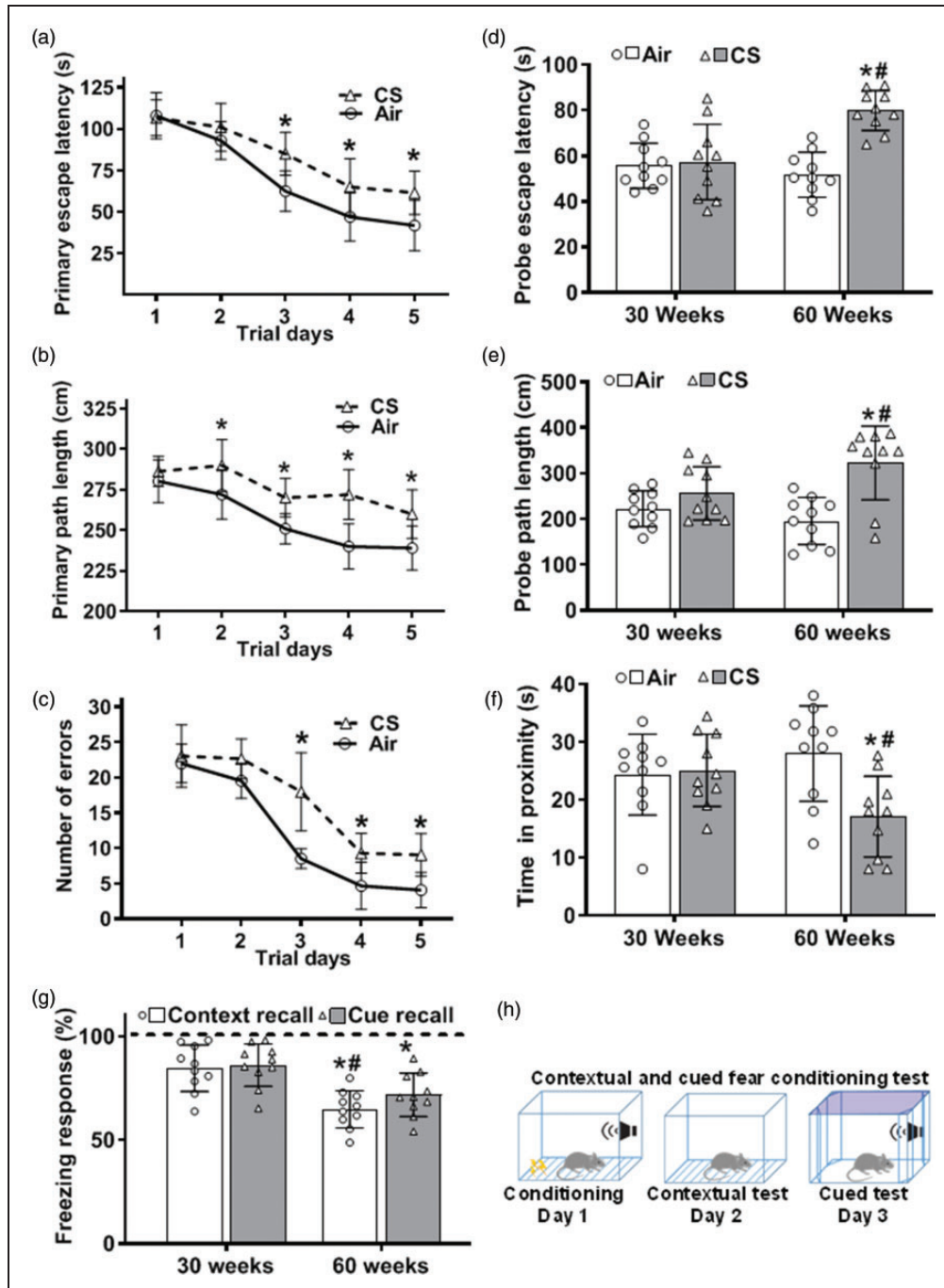


Figure 7. Cognitive impairment following cigarette smoke exposure. Mice were exposed to cigarette smoke (CS) or filtered air (Air) for 30 or 60 weeks. Spatial learning and memory were evaluated by Barnes maze (a–f). Contextual and cued fear memories were evaluated using contextual and cued fear conditioning test (g–h). (a–c) Acquisition phase at 60 weeks of CS. (d–f) Probe test at 30 and 60 weeks of exposure. (g) Freezing response during presentation of conditioning context (Context recall) and an auditory cue (Cue recall) on the second and third testing days as depicted in the bottom panel (h). Dotted line in (g) presents the freezing response of air-exposed control to the contextual and cued recall as 100%. CS data shown as bars is relative to the response shown as dotted line. At 30 weeks of exposure, there were no significant differences in all tested parameters. However, we observed cognitive impairment at 60 weeks of CS exposure, shown as longer escape latency (a) & (d), longer path length (b) & (e), higher number of errors and less time spent in proximity (c) & (f), and less times of freezing (g), compared to Air. Data are mean \pm SD with $n = 10$ per group. Analysis was done by two-way ANOVA followed by Bonferroni multiple comparison test. While CS exposure of 30 weeks was not sufficient to cause impairment, with 60 weeks of CS exposure both learning and memory were impaired. Data show statistical significance from: Air (*) and 30 weeks of CS exposure (#) at $p < 0.05$.

and cued fear conditioning tests showed that mouse freezing response was significantly decreased at 60 weeks of CSE compared to air-exposed control. This decrease in freezing response indicates that CSE decreased the ability of mice to learn and remember an association between environmental cues and aversive experiences. Thus, 60 weeks of CSE impaired both contextual fear and cued fear memories.

Discussion

The connection between CSE and CI has remained unclear due to variable results in human studies and the lack of comprehensive chronic studies in controlled animal models.^{44–47} Therefore, we investigated the effects of CSE on cerebrovascular function and cognition as well as their underlying mechanisms in our 60 week CSE mouse model that mimics chronic human smoking with similar blood nicotine/cotinine levels and exposure duration – life-span ratio.^{22,30} Our study demonstrates the temporal effects of CSE on the development of cognitive deficits and shows that CSE impairs spatial learning and memory. It is also the first to comprehensively assess the relationship between CSE and cognitive decline in otherwise healthy wild-type mice, with detailed identification of cerebrovascular and neuronal alterations relating to oxidative stress and inflammation.

Smoking-induced cardiovascular abnormalities and VED with oxidative damage and vascular inflammation have been hypothesized as a central cause of CS-induced disease, including that affecting the central nervous system.^{21,23,24,48} However, the temporal associations of CS-induced cardiovascular and cerebrovascular oxidative stress, and inflammation with the onset of CI were unknown. Therefore, we investigated these mechanisms and their association with cerebrovascular and neuronal injury and the subsequent onset of CI. Our findings demonstrate that CSE causes ROS-mediated vascular damage, VED, altered cerebral perfusion, and cerebrovascular injury with breakdown of the BBB. We also observe increased microglial activation and astrogliosis along with accumulation of A β and P-tau with the formation of neurofibrillary tangles. These vascular and neuronal events progressively increased with exposure duration, resulting in the onset of impaired cognition and memory (SI Figure S8).

Cerebrovascular dysfunction and elevated ROS generation have been associated with memory and learning impairments.^{49,50} Tobacco cigarette smoke contains high levels of free radicals, oxidants and, ROS that in turn trigger inflammation and VED.²² In the current study, vascular oxidative stress in the carotid artery and elevated blood pressure were observed at eight weeks of exposure followed by VED in the carotid

artery at 16 weeks of CSE. These systemic vascular effects of CSE are consistent with prior studies demonstrating the functional consequences of CSE on the aorta and mesenteric artery where loss of eNOS has been observed.^{18,22} In these prior studies, NOS uncoupling with loss of NO production and increase in superoxide led to degradation and depletion of eNOS.^{22,51} In our model, exposure duration correlated with the severity of vascular dysfunction and hypertension. Similarly, studies in the spontaneously hypertensive stroke-prone rat, the severity of cerebral small vessel disease correlates with the duration of hypertension and oxidative vascular injury with endothelial dysfunction preceding the onset of hypertension.^{52–54} Along with hypertension-induced neurovascular dysfunction, neuroinflammation occurs leading to the manifestations of cerebral small vessel disease and vascular CI.⁵⁵ We observe similar processes in CS-induced hypertension and CI. Starting at 30 weeks of CSE, a reduction in carotid flow secondary to increased resistance of the carotid circulation is seen. This elevated vascular resistance further correlates with eNOS depletion in the carotid artery and its distal cerebral microvessels. Taken together these findings would be expected to reduce cerebral perfusion that could further contribute to the onset of CI.

We also observed that CSE-induced carotid VED was associated with vascular oxidative injury as evidenced by increased lipid peroxidation and protein carbonylation in the carotid artery. These oxidative changes may be due to exposure of the vessels to CS-generated ROS. Cigarette smoke contains reactive compounds that can reduce molecular oxygen to produce superoxide, hydrogen peroxide, and hydroxyl radicals.⁵⁶ These radicals can initiate oxidative degradation of lipids in endothelial cells, leading to high levels of lipid peroxidation and increased ROS formation within the vasculature, which may overwhelm antioxidant defense mechanisms in vascular cells, triggering VED.⁵⁷ Moreover, CS-generated carbonyls have been shown to markedly increase carotid artery permeability, causing endothelial damage that can lead to VED.⁵⁸ Therefore, CS-induced oxidative stress through the generation of primary and secondary ROS is a key trigger of vascular injury, which can, in turn, lead to oxidative brain injury as depicted in SI Figure S8.

Since endothelial cells are central components of the neurovascular unit, forming the blood brain barrier (BBB) through their tight junctions, the combination of VED with inflammation and oxidative stress could lead to breakdown of the BBB.⁵⁹ Histological examination of the brain of CS-exposed mice showed alterations in the cerebral microvessels, with enlarged perivascular spaces and congestion. Loss of BBB integrity was observed with the leak of plasma proteins through the vessel walls to the surrounding brain

tissue. The tight junction proteins Occludin and Claudin-5 that are required for BBB integrity were found to be depleted in the endothelium of brain vessels. In association with these pathological events, neuroinflammation and neuronal oxidative stress occurred leading to secondary brain damage and CI.⁶⁰ Indeed, with CSE, oxidative brain injury was observed with increased superoxide generation, oxidative DNA damage and tyrosine nitration, indicative of hydroxyl radical and peroxynitrite generation. Furthermore, evidence of neuroinflammation was identified with increase in Iba1, a marker of microglia activation and GFAP another marker for astrogliosis.

Amyloid pathology is a central finding in neurodegenerative diseases and it is also associated with cerebrovascular diseases.⁶¹ During amyloidogenesis, amyloid precursor protein is cleaved into small A β fragments, mainly A β -40 and A β -42.^{62,63} A β -42 is the most harmful and insoluble fragment of A β with a faster aggregation tendency. It can initiate formation of insoluble amyloid aggregates that are further enlarged by A β -40 to form insoluble plaques.^{62,63} In our study, we observed increases in both A β forms in the brain homogenates of CS-exposed mice, with a higher increase in A β -42 than A β -40. Increased expression of total A β in cortical and hippocampal regions was also seen. This increase in A β and oxidative stress can upregulate tau phosphorylation, a well-known feature of neurodegenerative disease.⁶⁴ Phosphorylation of tau at serine 396 and 404 is an earlier marker that correlates with chronological disease progression and contributes to neurofibrillary tangle formation.⁶⁵ We observed that CSE increased P-tau in both the cortex and hippocampus. Similar results have been reported following exposure of wild-type rats and 3xTg-AD transgenic mice to CS.^{23,66} We also detected higher levels of ThioS-positive neurofibrillary aggregates that contain extracellular amyloid structures or paired helical filaments from tau phosphorylation.³⁶

In our model, vascular oxidative stress and elevated blood pressure were observed at 8 weeks, while increase in both P-tau and A β were only first seen after 16 weeks of CSE with further marked increase after 64 weeks of CSE. Therefore, we propose that p-tau and A β may be increased as a response to the vascular oxidative stress and inflammation in the brain with oxidative protein injury (SI Figure S8). These findings are in line with the recent critical revision of the amyloid cascade hypothesis and support the multi-factor complexity of cognitive impairment.⁶⁷ Consistent with our observations, in a human clinical case-control study that evaluated the effects of cigarette smoking on brain cerebrospinal biochemical parameters, elevations in A β 42 levels along with oxidative stress, neuroinflammation, and impaired neuroprotection was reported.³

In view of the prior controversy regarding the effects of cigarette smoking on cognition,^{1-4,68,69} we also assessed the effects of CSE on spatial learning and memory. While 30 weeks of CSE was insufficient to significantly impair learning or memory function, 60 weeks of exposure caused prominent deficits in spatial learning and short-term memory, as well as contextual and cued memory. The appearance of these cognitive and memory defects at 60 weeks, but not at 30 weeks, suggests that the progressive and cumulative oxidative and inflammatory stress with vascular and neurobiological changes must persist to manifest in cognitive and memory impairment.

In summary, our study has established a chronic model of CSE induced CI in otherwise healthy mice. It also details the temporal progression of the underlying pathological processes of CS-induced cerebrovascular and neuronal injury with their associated cognitive decline. Finally, it demonstrates the importance of cerebrovascular endothelial dysfunction, vascular oxidative stress and inflammation as critical pathological events in the development of CS-induced CI. Future mechanistic studies will be needed to determine the cause-effect relationship for each of these mechanisms and their precise role in the onset of CI. It will also be important to ascertain if sex-dependent differences occur. Our current model and observations pave the way for future studies utilizing genetically modified mice or specific pharmacological inhibitors to further unravel these mechanisms, their relative role in CS-induced CI and develop specific disease targeted therapeutics.

Study approval

This study was reviewed and approved by the Institutional Laboratory Animal Care and Use Committee (IACUC) and conformed to NIH Guidelines for Care and Use of Laboratory Animals.

Funding

The author(s) disclosed receipt of the following financial support for the research, authorship, and/or publication of this article: This work was supported by National Heart, Lung, and Blood Institute and American Lung Association Grants R01HL135648, R01HL131941, and GR120177 to J.L.Z. We acknowledge financial support from the Egyptian Ministry of Higher Education to M.G.E..

Acknowledgements

We thank Dr. Olga Kokiko-Cochran and Julie Fitzgerald of the Neuroscience Rodent Behavior Core for technical support and acknowledge core support from NINDS-P30NS045758. We also acknowledge use of the OSU-CCC Microscopy and Small Animal Imaging Resources.

Declaration of conflicting interests

The author(s) declared no potential conflicts of interest with respect to the research, authorship, and/or publication of this article.

Authors' contributions


J.L.Z. obtained funding for all this work. M.G.E., M.A.E., and J.L.Z. conceived and designed the research; M.G.E. performed experiments and analyzed data; M.G.E., M.A.E., Y. H., and J.L.Z. interpreted results of experiments, and drafted and edited the manuscript; M.G.E. prepared the Figures. All authors revised, critically discussed, and approved the data and the final version of the manuscript.

Supplementary material

Supplemental material for this article is available online.

ORCID iDs

Yousef Hannawi  <https://orcid.org/0000-0001-8614-3974>

Jay L Zweier  <https://orcid.org/0000-0002-9414-9150>

References

- Durazzo TC, Mattsson N and Weiner MW. and Alzheimer's Disease Neuroimaging I. Smoking and increased Alzheimer's disease risk: a review of potential mechanisms. *Alzheimers Dement* 2014; 10: S122–S145.
- Barnes DE and Yaffe K. The projected effect of risk factor reduction on Alzheimer's disease prevalence. *Lancet Neurol* 2011; 10: 819–828.
- Liu Y, Li H, Wang J, et al. Association of cigarette smoking with cerebrospinal fluid biomarkers of neurodegeneration, neuroinflammation, and oxidation. *JAMA Netw Open* 2020; 3: e2018777.
- Caldirola D, Daccò S, Grassi M, et al. Effects of cigarette smoking on neuropsychological performance in mood disorders: a comparison between smoking and nonsmoking inpatients. *J Clin Psychiatry* 2013; 74: e130–e136.
- Cervilla JA, Prince M and Mann A. Smoking, drinking, and incident cognitive impairment: a cohort community based study included in the gospel oak project. *J Neurol Neurosurg Psychiatry* 2000; 68: 622–626.
- Herbert LE, Scherr PA, Beckett LA, et al. Relation of smoking and low-to-moderate alcohol consumption to change in cognitive function: a longitudinal study in a defined community of older persons. *Am J Epidemiol* 1993; 137: 881–891.
- Ford AB, Mefrouche Z, Friedland RP, et al. Smoking and cognitive impairment: a population-based study. *J Am Geriatr Soc* 1996; 44: 905–909.
- Wang HX, Fratiglioni L, Frisoni GB, et al. Smoking and the occurrence of Alzheimer's disease: cross-sectional and longitudinal data in a population-based study. *Am J Epidemiol* 1999; 149: 640–644.
- McDonald WM. Overview of neurocognitive disorders. *Focus (Am Psychiatr Publ)* 2017; 15: 4–12.
- Sousa RM, Ferri CP, Acosta D, et al. Contribution of chronic diseases to disability in elderly people in countries with low and Middle incomes: a 10/66 dementia research group population-based survey. *Lancet* 2009; 374: 1821–1830.
- Kim HA, Miller AA, Drummond GR, et al. Vascular cognitive impairment and Alzheimer's disease: role of cerebral hypoperfusion and oxidative stress. *Naunyn Schmiedebergs Arch Pharmacol* 2012; 385: 953–959.
- Liu H and Zhang J. Cerebral hypoperfusion and cognitive impairment: the pathogenic role of vascular oxidative stress. *Int J Neurosci* 2012; 122: 494–499.
- Panza F, Solfrizzi V, Colacicco AM, et al. Cerebrovascular disease in the elderly: lipoprotein metabolism and cognitive decline. *Aging Clin Exp Res* 2006; 18: 144–148.
- DeCarli C, Miller BL, Swan GE, et al. Cerebrovascular and brain morphologic correlates of mild cognitive impairment in the national heart, lung, and blood institute twin study. *Arch Neurol* 2001; 58: 643–647.
- Toda N and Okamura T. Cigarette smoking impairs nitric oxide-mediated cerebral blood flow increase: implications for Alzheimer's disease. *J Pharmacol Sci* 2016; 131: 223–232.
- Chen CA, De Pascali F, Basye A, et al. Redox modulation of endothelial nitric oxide synthase by glutaredoxin-1 through reversible oxidative post-translational modification. *Biochemistry* 2013; 52: 6712–6723.
- Chen C-A, Wang T-Y, Varadharaj S, et al. S-glutathionylation uncouples eNOS and regulates its cellular and vascular function. *Nature* 2010; 468: 1115–1118.
- Crow JP and Beckman JS. Reactions between nitric oxide, superoxide, and peroxynitrite: footprints of peroxynitrite in vivo. In: Ignarro L and Murad F (eds) *Advances in pharmacology*. Amsterdam: Academic Press, 1995, pp. 17–43.
- Wardlaw JM, Smith C and Dichgans M. Mechanisms of sporadic cerebral small vessel disease: insights from neuroimaging. *Lancet Neurol* 2013; 12: 483–497.
- Zlokovic BV. The blood-brain barrier in health and chronic neurodegenerative disorders. *Neuron* 2008; 57: 178–201.
- Starke Robert M, Thompson John W, Ali Muhammad S, et al. Cigarette smoke initiates oxidative Stress-Induced cellular phenotypic modulation leading to cerebral aneurysm pathogenesis. *Arterioscler Thromb Vasc Biol* 2018; 38: 610–621.
- El-Mahdy MA, Abdelghany TM, Hemann C, et al. Chronic cigarette smoke exposure triggers a vicious cycle of leukocyte and endothelial-mediated oxidant stress that results in vascular dysfunction. *Am J Physiol Heart Circ Physiol* 2020; 319: H51–H65.
- Moreno-Gonzalez I, Estrada LD, Sanchez-Mejias E, et al. Smoking exacerbates amyloid pathology in a mouse model of Alzheimer's disease. *Nat Commun* 2013; 4: 1495.
- Talukder MA, Johnson WM, Varadharaj S, et al. Chronic cigarette smoking causes hypertension, increased oxidative stress, impaired NO bioavailability, endothelial dysfunction, and cardiac remodeling in mice. *Am J Physiol Heart Circ Physiol* 2011; 300: H388–96.

25. Church DF and Pryor WA. Free-radical chemistry of cigarette smoke and its toxicological implications. *Environ Health Perspect* 1985; 64: 111–126.
26. Caia GL, Efimova OV, Velayutham M, et al. Organ specific mapping of in vivo redox state in control and cigarette smoke-exposed mice using EPR/NMR co-imaging. *J Magn Reson* 2012; 216: 21–27.
27. Cafè C, Torri C, Gazzaniga L, et al. Oxygen radicals in central nervous system injury. *Minerva Anesthesiol* 1994; 60: 517–521.
28. Floyd RA and Hensley K. Oxidative stress in brain aging. Implications for therapeutics of neurodegenerative diseases. *Neurobiol Aging* 2002; 23: 795–807.
29. Percie Du Sert N, Hurst V, Ahluwalia A, et al. The ARRIVE guidelines 2.0: updated guidelines for reporting animal research. *J Cereb Blood Flow Metab* 2020; 40: 1769–1777.
30. El-Mahdy MA, Mahgoup EM, Ewees MG, et al. Long-term electronic cigarette exposure induces cardiovascular dysfunction similar to tobacco cigarettes: role of nicotine and exposure duration. *Am J Physiol Heart Circ Physiol* 2021; 320: H2112–H2129.
31. Yamazaki H, Horiuchi K, Takano R, et al. Human blood concentrations of cotinine, a biomonitoring marker for tobacco smoke, extrapolated from nicotine metabolism in rats and humans and physiologically based pharmacokinetic modeling. *Int J Environ Res Public Health* 2010; 7: 3406–3421.
32. Zweier JL, Shalaan MT, Samouilov A, et al. Whole body electronic cigarette exposure system for efficient evaluation of diverse inhalation conditions and products. *Inhal Toxicol* 2020; 32: 477–486.
33. El-Mahdy MA, Ewees MG, Eid MS, et al. Electronic cigarette exposure causes vascular endothelial dysfunction due to NADPH oxidase activation and eNOS uncoupling. *Am J Physiol Heart Circ Physiol* 2022; 322: H549–H567.
34. Gao S, Ho D, Vatner DE, et al. Echocardiography in mice. *Curr Protoc Mouse Biol* 2011; 1: 71–83.
35. Jeong JW, Park OK, Park YK, et al. Changes of the carotid artery doppler flow velocity pattern after sublingual nitroglycerin in patients with hypertension. *Korean J Intern Med* 1998; 13: 22–26.
36. Santa-María I, Pérez M, Hernández F, et al. Characteristics of the binding of thioflavin S to tau paired helical filaments. *J Alzheimers Dis* 2006; 9: 279–285.
37. Groenning M. Binding mode of thioflavin T and other molecular probes in the context of amyloid fibrils – current status. *J Chem Biol* 2010; 3: 1–18.
38. Kalaria RN, Kenny RA, Ballard CG, et al. Towards defining the neuropathological substrates of vascular dementia. *J Neurol Sci* 2004; 226: 75–80.
39. Rosenfeld CS and Ferguson SA. Barnes maze testing strategies with small and large rodent models. *J Vis Exp* 2014; e51194.
40. Shoji H, Takao K, Hattori S, et al. Contextual and cued fear conditioning test using a video analyzing system in mice. *J Vis Exp* 2014; 50871.
41. Zhao H, Kalivendi S, Zhang H, et al. Superoxide reacts with hydroethidine but forms a fluorescent product that is distinctly different from ethidium: potential implications in intracellular fluorescence detection of superoxide. *Free Radic Biol Med* 2003; 34: 1359–1368.
42. Duarte AI, Candeias E, Alves IN, et al. Liraglutide protects against brain amyloid- β (1-42) accumulation in female mice with early Alzheimer’s disease-like pathology by partially rescuing oxidative/nitrosative stress and inflammation. *Int J Mol Sci* 2020; 21: 1746.
43. Tiwari SS, Mizuno K, Ghosh A, et al. Alzheimer-related decrease in CYFIP2 links amyloid production to tau hyperphosphorylation and memory loss. *Brain* 2016; 139: 2751–2765.
44. Graves AB, van Duijn CM, Chandra V, et al. Alcohol and tobacco consumption as risk factors for Alzheimer’s disease: a collaborative re-analysis of case-control studies. EURODEM risk factors research group. *Int J Epidemiol* 1991; 20 Suppl 2: S48–57.
45. Ulrich J, Johansson-Locher G, Seiler WO, et al. Does smoking protect from Alzheimer’s disease? Alzheimer-type changes in 301 unselected brains from patients with known smoking history. *Acta Neuropathol* 1997; 94: 450–454.
46. Hellström-Lindahl E, Mousavi M, Ravid R, et al. Reduced levels of abeta 40 and abeta 42 in brains of smoking controls and Alzheimer’s patients. *Neurobiol Dis* 2004; 15: 351–360.
47. Tyas SL, White LR, Petrovitch H, et al. Mid-life smoking and late-life dementia: the Honolulu-Asia aging study. *Neurobiol Aging* 2003; 24: 589–596.
48. Münzel T, Hahad O, Kuntic M, et al. Effects of tobacco cigarettes, e-cigarettes, and waterpipe smoking on endothelial function and clinical outcomes. *Eur Heart J* 2020; 41: 4057–4070.
49. Kruk-Slomka M, Boguszewska-Czubara A, Slomka T, et al. Correlations between the memory-related behavior and the level of oxidative stress biomarkers in the mice brain, provoked by an acute administration of CB receptor ligands. *Neural Plast* 2016; 2016: 9815092.
50. Shabir O, Berwick J and Francis SE. Neurovascular dysfunction in vascular dementia, Alzheimer’s and atherosclerosis. *BMC Neurosci* 2018; 19: 62.
51. Abdelghany TM, Ismail RS, Mansoor FA, et al. Cigarette smoke constituents cause endothelial nitric oxide synthase dysfunction and uncoupling due to depletion of tetrahydrobiopterin with degradation of GTP cyclohydrolase. *Nitric Oxide* 2018; 76: 113–121.
52. Hannawi Y, Caceres E, Ewees MG, et al. Characterizing the neuroimaging and histopathological correlates of cerebral small vessel disease in spontaneously hypertensive stroke-prone rats. *Front Neurol* 2021; 12: 740298.
53. Hannawi Y, Ewees MG, Moore JT, et al. Characterizing CD38 expression and enzymatic activity in the brain of spontaneously hypertensive stroke-prone rats. *Front Pharmacol* 2022; 13: 881708.
54. Rajani RM, Quick S, Ruigrok SR, et al. Reversal of endothelial dysfunction reduces white matter

- vulnerability in cerebral small vessel disease in rats. *Sci Transl Med* 2018; 10: eaam9507.
55. Hannawi Y. Cerebral small vessel disease: a review of the pathophysiological mechanisms. *Transl Stroke Res* 2023. DOI: 10.1007/s12975-023-01195-9.
 56. Valavanidis A, Vlachogianni T and Fiotakis K. Tobacco smoke: involvement of reactive oxygen species and stable free radicals in mechanisms of oxidative damage, carcinogenesis and synergistic effects with other respirable particles. *Int J Environ Res Public Health* 2009; 6: 445–462.
 57. Michael Pittilo R. Cigarette smoking, endothelial injury and cardiovascular disease. *Int J Exp Pathol* 2000; 81: 219–230.
 58. Mullick AE, McDonald JM, Melkonian G, et al. Reactive carbonyls from tobacco smoke increase arterial endothelial layer injury. *Am J Physiol Heart Circ Physiol* 2002; 283: H591–7.
 59. Schaeffer S and Iadecola C. Revisiting the neurovascular unit. *Nat Neurosci* 2021; 24: 1198–1209.
 60. Takata F, Nakagawa S, Matsumoto J, et al. Blood-Brain barrier dysfunction amplifies the development of neuroinflammation: Understanding of cellular events in brain microvascular endothelial cells for prevention and treatment of BBB dysfunction. *Front Cell Neurosci* 2021; 15: 661838.
 61. Bos I, Verhey FR, Ramakers IHGB, et al. Cerebrovascular and amyloid pathology in predementia stages: the relationship with neurodegeneration and cognitive decline. *Alzheimers Res Ther* 2017; 9: 101.
 62. Murphy MP and LeVine H 3rd. Alzheimer's disease and the amyloid-beta peptide. *J Alzheimers Dis* 2010; 19: 311–323.
 63. Stine WB, Jungbauer L, Yu C, et al. Preparing synthetic A β in different aggregation states. *Methods Mol Biol* 2011; 670: 13–32.
 64. Zheng WH, Bastianetto S, Mennicken F, et al. Amyloid beta peptide induces tau phosphorylation and loss of cholinergic neurons in rat primary septal cultures. *Neuroscience* 2002; 115: 201–211.
 65. Mondragon-Rodriguez S, Perry G, Luna-Munoz J, et al. Phosphorylation of tau protein at sites ser(396-404) is one of the earliest events in Alzheimer's disease and down syndrome. *Neuropathol Appl Neurobiol* 2014; 40: 121–135.
 66. Ho Y-S, Yang X, Yeung S-C, et al. Cigarette smoking accelerated brain aging and induced Pre-Alzheimer-like neuropathology in rats. *Plos ONE* 2012; 7: e36752.
 67. Kepp KP, Robakis NK, Høilund-Carlsen PF, et al. The amyloid Cascade hypothesis: an updated critical review. *Brain* 2023; 146: 3969–3990.
 68. Cataldo JK, Prochaska JJ and Glantz SA. Cigarette smoking is a risk factor for Alzheimer's disease: an analysis controlling for tobacco industry affiliation. *J Alzheimers Dis* 2010; 19: 465–480.
 69. Bachman DL, Green RC, Benke KS, et al. Comparison of Alzheimer's disease risk factors in white and African American families. *Neurology* 2003; 60: 1372–1374.